An accurate analytic potential function for ground-state N_2 from a direct-potential-fit analysis of spectroscopic data

Robert J. Le Roy,[a] Yiye Huang, and Calvin Jary
Department of Chemistry, University of Waterloo, Waterloo, Ontario N2L 3G1, Canada

(Received 29 June 2006; accepted 21 August 2006; published online 24 October 2006)

Two types of combined-isotopologue analysis have been performed on an extensive spectroscopic data set for ground-state N_2 involving levels up to $v=19$, which is bound by half the well depth. Both a conventional Dunham-type analysis and a direct-potential-fit (DPF) analysis represent the data within (on average) the estimated experimental uncertainties. However, the Dunham-type parameters do not yield realistic predictions outside the range of the data used in the analysis, while the potential function obtained from the DPF treatment yields quantum mechanical accuracy over the data region and realistic predictions of the energies and properties of unobserved higher vibrational levels. Our DPF analysis also introduces a compact new analytic potential function form which incorporates the two leading inverse-power terms in the long-range potential. © *2006 American Institute of Physics*. [DOI: 10.1063/1.2354502]

I. INTRODUCTION

The fact that N_2 is the most abundant component of the Earth's atmosphere makes its optical and other properties topics of great importance. However, in spite of many decades of study, there is no well-accepted accurate and portable potential energy function for its ground $X\,^1\Sigma_g^+$ state. While numerous spectroscopic studies have been performed on this system over the past century, the results were usually analyzed in a piecemeal manner and empirical potential energy functions have only been obtained using the first-order semiclassical Rydberg-Klein-Rees (RKR) procedure.[1] However, such potentials lack full quantum mechanical accuracy, their pointwise representation makes them inconvenient to work with, and they incorporate no means for extrapolating sensibly beyond the range of the data used in the spectroscopic data analysis. While a number of high quality *ab initio* studies have been reported for this system,[2–5] none of them achieve full spectroscopic accuracy. Moreover, there exists no comprehensive set of molecular band constants or Dunham-type expansion coefficients which attempt to represent all of the available data.

In view of the above, the present work began with a critical assessment of the spectroscopic data for this system. The resulting consolidated data set is a combination of Raman and electric quadrupole vibration-rotation data with a grid of term values determined from electronic spectra. These data were first analyzed in a Dunham-type combined-isotopologue "parameter-fit" analysis which yields a recommended set of conventional molecular constants and Born-Oppenheimer breakdown (BOB) parameters. A direct-potential-fit (DPF) analysis was then used to obtain a compact analytic potential function and associated BOB functions for this system.

[a]Electronic mail: leroy@uwaterloo.ca

II. DATA USED IN THE ANALYSIS

Because molecular nitrogen lacks a dipole moment, many studies of it have utilized Raman spectroscopy.[6–16] The earliest such work was reported by Rasetti in 1929.[6] Later works by Stoicheff[7] in 1954 and Butcher *et al.*[8] in 1971 yielded improved values of the the leading ground-state rotational constants B_0 and D_0; however, their data have been supplanted by more recent work. The first Raman measurements which included data for the minor isotopologues $^{14,15}N_2$ and $^{15,15}N_2$ were the 1974 results of Bendtsen.[9] Although his fundamental band vibration-rotation data have been superseded by more accurate later work,[15,16] his pure rotation data for the three isotopologues are a central component of the present analysis.

Since 1980, coherent anti-Stokes stimulated Raman spectroscopy (CARS) techniques have been successfully applied to N_2 by a number of groups.[10–14] In 1980, Gilson *et al.*[10] obtained vibrational Q-branch data for all three isotopologues which extend to $J=48$ for the fundamentals and to $J=30$ for the hot bands. However, their $^{14,15}N_2$ hot-band and $^{15}N_2$ fundamental-band lines have large systematic discrepancies with more recent work, and so were omitted from our analyses. Moreover, to achieve approximate consistency with results from other sources, the reported uncertainties associated with their hot-band results for $^{14,14}N_2$ and all remaining results for $^{14,15}N_2$ and $^{15,15}N_2$ had to be doubled to $\pm 0.02\ \mathrm{cm}^{-1}$. Lavorel *et al.* reported making Q-branch CARS $\Delta v=1$ measurements for v up to 14.[11,12] Unfortunately, the line positions for the hot bands were not reported, and those for the fundamental band are displaced by ca. $0.05\ \mathrm{cm}^{-1}$ from more recent values, so none of those results could be used in the present work. That same group later reported high resolution measurements of the fundamental and first hot band extending to relatively high J values,[13] which were utilized in the present analyses. In more recent work, Orlov *et al.*[14] reported CARS measurements of $\Delta v=1$ Q-branch transitions for $v=1-7$ of $^{14,14}N_2$ and $v=0-6$ of $^{15,15}N_2$. The

TABLE I. Spectroscopic data for ground-state N_2 used in the present analysis.

Species	Type	Δv	v''	J''_{max}	unc./cm^{-1}	No. of lines	Source	Year
$^{14,14}N_2$	Raman	0	0	18	0.001	19	Bendtsen[a]	1974
	CARS	1	0	48	0.01	42	Gilson *et al.*[b]	1980
	CARS	1	1	30	0.02	24	Gilson *et al.*[b]	1980
	Quadrupole	1	0	21	0.004 3	18	Reuter *et al.*[c]	1986
	CARS	1	0	47	0.001 3	15	Tabyoui *et al.*[d]	1990
	CARS	1	1	26	0.002 2	24	Tabyoui *et al.*[d]	1990
	Quadrupole	1	0	22	0.000 6	19	Rinslandet *et al.*[e]	1991
	CARS	1	1	14	0.001 4	15	Orlov *et al.*[f]	1997
	CARS	1	2	20	0.001 8	21	Orlov *et al.*[f]	1997
	CARS	1	3	20	0.004 1	21	Orlov *et al.*[f]	1997
	CARS	1	4	18	0.001 4	19	Orlov *et al.*[f]	1997
	CARS	1	5	17	0.001 6	16	Orlov *et al.*[f]	1997
	CARS	1	6	22	0.003 5	21	Orlov *et al.*[f]	1997
	CARS	1	7	12	0.002 2	6	Orlov *et al.*[f]	1997
	Raman	1	0	24	0.000 54	56	Bendtsen and Rasmussen[g]	2000
	Electronic	n/a	0–19	16–32	0.07	525	Roncin *et al.*[h]	1999
$^{14,15}N_2$	Raman	0	0	19	0.001	18	Bendtsen[a]	1974
	CARS	1	0	48	0.02	37	Gilson *et al.*[b]	1980
	Raman	1	0	26	0.000 54	60	Bendtsen[i]	2001
$^{15,15}N_2$	Raman	0	0	21	0.001	20	Bendtsen[a]	1974
	CARS	1	1	29	0.02	11	Gilson *et al.*[b]	1980
	CARS	1	0	25	0.001 0	25	Orlov *et al.*[f]	1997
	CARS	1	1	27	0.001 6	27	Orlov *et al.*[f]	1997
	CARS	1	2	25	0.001 7	25	Orlov *et al.*[f]	1997
	CARS	1	3	25	0.004 3	24	Orlov *et al.*[f]	1997
	CARS	1	4	23	0.003 0	21	Orlov *et al.*[f]	1997
	CARS	1	5	25	0.003 2	25	Orlov *et al.*[f]	1997
	CARS	1	6	25	0.001 8	12	Orlov *et al.*[f]	1997
	Raman	1	0	25	0.0005 6	55	Bendtsen[i]	2001

[a]Reference 9.
[b]Reference 10.
[c]Reference 17.
[d]Reference 13.
[e]Reference 18.
[f]Reference 14.
[g]Reference 15.
[h]Reference 25.
[i]Reference 16.

present analysis used essentially all of their data, weighed according to their reported uncertainties, omitting only the handful of lines which they identified as being relatively unreliable.

The most recent Raman data for this system are the "conventional" incoherent Fourier-transform fundamental-band measurements reported by Bendtsen and Rasmussen[15] and Bendtsen[16] in 2000 and 2001. These results are particularly useful because they include *O*- and *S*-branch measurements, while the reliable CARS data consist only of *Q*-branch transitions. Following Bendtsen and Rasmussen,[15] the transition energies in their Table I were shifted by the addition of the quantity of 0.0025 cm^{-1}.

Additional high resolution fundamental-band data for $^{14,14}N_2$ were obtained in direct absorption experiments in which the transitions were driven by the radial dependence of the molecular quadrupole moment.[17,18]

Over the years there have been a wide range of studies of the electronic spectra of N_2, and a thorough evaluation of those results would be a massive undertaking (for some of the more recent work involving the ground state, see, e.g., Refs. 19–25). Fortunately, such a review was recently reported by Roncin *et al.*,[25] who summarized their results in the form of a list of term values for vibrational levels $v=0-19$ and J sublevels ranging up to 16–32. While no average uncertainty was reported for these 525 term values,[26] good internal consistency among those data and between them and the Raman and quadrupole absorption results was obtained if their uncertainties were assumed to be ± 0.07 cm^{-1}.

An overview of the data used in the present analysis is presented in Table I; for each data group listed there, the quantity "unc." is the average of the uncertainties used to weigh those data in our fits. Except as noted above, the uncertainties used here were those given in the original papers. A complete listing of the data used in this study may be obtained from the journal's online archive[27] or from the authors.

In the analyses reported below, the quality of the fit of an M-parameter model to N experimental data $y_{obs}(i)$ with uncertainties $u(i)$, which yield the predicted quantities $y_{calc}(i)$, is indicated by the value of the dimensionless root mean square (rms) deviation,

$$\overline{dd} \equiv \mathrm{DRMSD} = \left\{ \frac{1}{N} \sum_{i=1}^{N} \left[\frac{y_{\mathrm{calc}}(i) - y_{\mathrm{obs}}(i)}{u(i)} \right]^2 \right\}^{1/2} \quad (1)$$

or by the dimensionless standard error, $\mathrm{DSE} \equiv \bar{\sigma}_f = \sqrt{N/(N-M)}\,\overline{dd}$. A "good" fit is one which yields $\overline{dd}$ and $\bar{\sigma}_f$ values close to unity, since a $\overline{dd}$ value of (say) 3.7 would mean that on average the predictions of the model disagree with the input data by 3.7 times the estimated experimental uncertainties. Note, however, that converged values larger than unity may also reflect the fact that the experimental uncertainties assigned to the data were too small.

III. PARAMETER-FIT ANALYSIS

In a parameter-fit analysis, the observed transition energies are fitted to analytic expressions for the level energies as functions of the vibrational and rotational quantum numbers v and J. Such fits should also take account of level splittings (e.g., due to Λ doubling or $^2\Sigma$ splittings) and isotope shift effects, as appropriate. In the present fits, the level energies for all isotopologues were represented by a single set of Dunham $Y_{l,m}$ coefficients plus two BOB parameters. Using the formulation of Ref. 28, the vibration-rotation energies for isotopologue α in a $^1\Sigma$ electronic state are written as

$$\begin{aligned} E_{v,J}^{(\alpha)} &= \sum_{m=0}^{m_{\max}} \sum_{l=0}^{l_{\max}(m)} Y_{l,m}^{(\alpha)} \left(v + \frac{1}{2} \right)^l [J(J+1)]^m \\ &= \sum_{m=0}^{m_{\max}} \sum_{l=0}^{l_{\max}(m)} \left(\frac{\mu_1}{\mu_\alpha} \right)^{m+l/2} \left\{ Y_{l,m}^{(1)} + \frac{\Delta M_A^{(\alpha)}}{M_A^{(\alpha)}} \delta_{l,m}^{A} \right. \\ &\quad \left. + \frac{\Delta M_B^{(\alpha)}}{M_B^{(\alpha)}} \delta_{l,m}^{B} \right\} \left(v + \frac{1}{2} \right)^l [J(J+1)]^m, \end{aligned} \quad (2)$$

in which the $Y_{l,m}^{(1)}$ are the standard Dunham parameters for the chosen reference isotopologue ($\alpha=1$, here $^{14,14}N_2$), $Y_{0,0}^{(1)}=0$, $M_A^{(\alpha)}$ is the mass of atom A in isotopologue α, μ_α is the reduced mass of the two atoms forming that isotopologue, and $\Delta M_A^{(\alpha)} = M_A^{(\alpha)} - M_A^{(1)}$ is the difference between the masses of atom A in isotopologue α and in the reference isotopologue.

The BOB coefficients $\delta_{l,m}^{A/B}$ appearing in Eq. (2) may only be determined in a combined analysis of data for two or more isotopologues. Since N_2 is electronically homonuclear, the conventional Dunham coefficients for the minor isotopologues $^{14,15}N_2$ and $^{15,15}N_2$ are defined as

$$Y_{l,m}^{(\alpha)} = \left(\frac{\mu_1}{\mu_\alpha} \right)^{m+l/2} \left\{ Y_{l,m}^{\{14,14\}} + \left(\frac{\Delta M_{\mathrm{N}_a}^{(\alpha)}}{M_{\mathrm{N}_a}^{(\alpha)}} + \frac{\Delta M_{\mathrm{N}_b}^{(\alpha)}}{M_{\mathrm{N}_b}^{(\alpha)}} \right) \delta_{l,m}^{\mathrm{N}} \right\}, \quad (3)$$

in which N_a and N_b are the two nitrogen atoms forming the molecule. The parameter-fit analysis reported herein was performed using program DPARFIT.[29]

After some experimentation, an optimal Dunham-type description of the $X\,^1\Sigma_g^+$ state of N_2 was obtained with $m_{\max}=2$ and $l_{\max}(m)=\{5,3,1\}$ for $m=0-2$, respectively, for the $Y_{l,m}^{(^{14,14}\mathrm{N}_2)}$ coefficients and $m_{\max}=0$ with $l_{\max}(m)=\{2\}$ for the $\delta_{l,m}^{\mathrm{N}}$ BOB coefficients. This fit yielded $\overline{dd}=1.375$. The resulting parameter values are presented in Table II, together with the 95% confidence limit (approximately "2σ") uncertainties in the 13 fitted molecular parameters and the corresponding $Y_{l,m}$ parameters for the minor isotopologues generated from Eq. (3). The numbers of significant digits shown for the fitting parameters were determined by the sequential rounding and refitting procedure of Ref. 30, while the numbers of digits shown for the $^{14,15}N_2$ and $^{15,15}N_2$ parameters were determined by its "sensitivity rounding" criterion.[30] Somewhat smaller $\overline{dd}$ values can be obtained by allowing for additional BOB parameters, but the fact that the magnitudes of some of the resulting $\delta_{l,m}^{\mathrm{N}}$ constants are larger than the corresponding $Y_{l,m}^{(1)}$ coefficients suggests that this "improvement" is an artifact reflecting the fact that such unconstrained polynomial fits can hide systematic discrepancies in the data.

TABLE II. Recommended spectroscopic constants for ground-state N_2, all with units of cm^{-1}; for this fit, $\overline{dd}=1.375$. The numbers in parentheses represent 95% confidence limit uncertainties in the last digits shown.

Constant	$^{14,14}N_2$	$^{14,15}N_2$	$^{15,15}N_2$
$Y_{1,0}$	2358.533 73(87)	2319.007 90	2278.796 79
$Y_{2,0}$	−14.300 56(60)	−13.825 105	−13.349 663
$10^4 Y_{3,0}$	−65.22(140)	−61.996	−58.827
$10^4 Y_{4,0}$	0.60(12)	0.560 8	0.522 9
$10^4 Y_{5,0}$	−0.071 5(35)	−0.065 71	−0.060 20
$Y_{0,1}$	1.998 259(6)	1.931 84 84	1.865 437 7
$Y_{1,1}$	−0.017 324 3(17)	−0.016 467 88	−0.015 626 05
$10^5 Y_{2,1}$	−2.27(7)	−2.122	−1.978
$10^5 Y_{3,1}$	−0.053(5)	−0.048 7	−0.044 6
$10^7 Y_{0,2}$	−57.5(2)	−53.742	−50.110
$10^7 Y_{1,2}$	−0.098(8)	−0.090 1	−0.082 5
$\delta_{1,0}^{\mathrm{N}}$	−0.040(3)		
$\delta_{2,0}^{\mathrm{N}}$	0.002 9(7)		

It is interesting to note that although the vibrational levels considered in the present analysis extend from $v=0$ to 19, which is half the well depth, only relatively low-order Dunham polynomials (of orders 5 and 3) were required to fit the vibrational energies and inertial rotational constants for those levels. We also found that the BOB parameters $\delta_{l,m}^{\mathrm{N}}$ had a significant impact on the analysis. In particular, if the vibrational BOB coefficients $\delta_{l,0}^{\mathrm{N}}$ were omitted, $\overline{dd}$ increases by over 50% to 2.11. Thus, BOB effects are clearly nonnegligible for N_2.

IV. POTENTIAL-FIT ANALYSIS

A. Methodology and potential function forms

The conventional Dunham parameters for each isotopologue (see Table II) may be used in the familiar RKR inversion procedure[1,31] to generate a potential energy curve for each species. However, the resulting pointwise potentials are not the most convenient to work with, and the discrepancies between the first-order semiclassical basis of the RKR procedure and the exact quantal methods usually used for calculations utilizing such potentials can give rise to significant errors in calculated system properties, especially for hydrides and other species of small reduced mass. Moreover, empirical Dunham-type polynomial level energy expressions such

as Eq. (2) are well known to be unable to provide realistic predictions outside the range of the data used to determine them.

In view of the above, it has become increasingly common to perform spectroscopic data analyses using fully quantum mechanical DPF methods. In this approach, the observed level energy spacings are fitted directly to the difference between eigenvalues obtained by solving the effective radial Schrödinger equation, written here for the case of a $^1\Sigma$ electronic state,[32,33]

$$\left\{-\frac{\hbar^2}{2\mu_\alpha}\frac{d^2}{dr^2}+[V_{\rm ad}^{(1)}(r)+\Delta V_{\rm ad}^{(\alpha)}(r)] + \frac{\hbar^2 J(J+1)}{2\mu_\alpha r^2}[1+g^{(\alpha)}(r)]\right\}\psi_{v,J}(r)=E_{v,J}\psi_{v,J}(r), \quad (4)$$

in which $V_{\rm ad}^{(1)}(r)$ is the total effective adiabatic internuclear potential for the selected reference isotopologue, $\Delta V_{\rm ad}^{(\alpha)}(r)$ is the *difference* between the effective adiabatic potential for isotopologue α and that for the reference species ($\alpha=1$), and $g^{(\alpha)}(r)$ is the nonadiabatic centrifugal-potential correction function for isotopologue α.

In the present work, three models were considered for the effective adiabatic potential for $^{14,14}N_2$. The first is the "expanded Morse oscillator" (EMO or EMO$_p$) function, which has the form

$$V_{\rm EMO}(r)=\mathfrak{D}_e[1-e^{-\phi(r)(r-r_e)}]^2 \quad (5)$$

in which $\mathfrak{D}_e$ is the well depth, r_e the equilibrium distance, and the exponent coefficient is expressed as a simple power series expansion,

$$\phi(r)=\phi_{\rm EMO}(r)=\sum_{i=0}^{N}\phi_i y_p(r)^i, \quad (6)$$

in terms of a particular version of a generalized radial variable introduced by Šurkus *et al.*,[34]

$$y_p(r)=\frac{r^p-r_e^p}{r^p+r_e^p}. \quad (7)$$

Previous work has shown (see also Sec. IV B) that defining the exponent coefficient $\phi(r)$ as an expansion in the variable $y_p(r)$ for some appropriate small integer value of p which is greater than 1 (say, $p=2-4$) greatly reduces the propensity for the resulting potential function to exhibit nonphysical behavior (e.g., turnover) at distances outside the radial interval to which the data are sensitive.[35–37]

As discussed elsewhere,[35,37,38] setting $p>1$ in the definition of $y_p(r)$ does not always resolve extrapolation problems at small r. However, it was found that such residual extrapolation problems could usually be resolved by allowing the power series in Eq. (6) to have a lower order for $r \leqslant r_e$ than for $r>r_e$,

$$\phi_{\rm EMO}(r)=\sum_{i=0}^{N_S}\phi_i y_p(r)^i \quad \text{for } r\leqslant r_e, \quad (8)$$

$$\phi_{\rm EMO}(r)=\sum_{i=0}^{N_L}\phi_i y_p(r)^i \quad \text{for } r>r_e. \quad (9)$$

Thus, the use of different polynomial orders for $\phi(r)$ at short (N_S) and long range (N_L) is another option of this model. Normally $N_S \leqslant N_L$, because the portion of the data region for which $r\leqslant r_e$ is much narrower than that for $r>r_e$. Note too that for powers $i\leqslant \min\{N_S,N_L\}$, the coefficients ϕ_i of the "inner" and "outer" exponent expansions of Eqs. (8) and (9), are identical. A dramatic illustration of the utility of using mixed exponent polynomial orders ($N_S\neq N_L$) is seen in Fig. 2 of Ref. 37.

The EMO potential form has been used successfully in a number of demanding data analyses involving both "normal" single-well potentials[39–41] and states whose potential functions have an additional "ripple."[38] However, the fact that $[\mathfrak{D}_e-V_{\rm EMO}(r)]$ dies off exponentially at large r means that it will provide a poor description of the behavior of a potential energy function as it approaches its asymptote. This concern is addressed by either the "Morse/Lennard-Jones" (MLJ or MLJ$_p$) functional form,[42–44]

$$V_{\rm MLJ}(r)=\mathfrak{D}_e\left\{1-\left(\frac{r_e}{r}\right)^n e^{-\phi(r)y_p(r)}\right\}^2, \quad (10)$$

or our new "Morse/long-range" (MLR or MLR$_p$) potential form,[45]

$$V_{\rm MLR}(r)=\mathfrak{D}_e\left\{1-\left(\frac{r_e}{r}\right)^n\left[\frac{1+R_{m,n}/r^{m-n}}{1+R_{m,n}/r_e^{m-n}}\right]e^{-\phi(r)y_p(r)}\right\}^2, \quad (11)$$

in both of which $\mathfrak{D}_e$ is the well depth, r_e is the equilibrium internuclear distance, and the exponent coefficient $\phi(r)=\phi_{\rm MLJ}(r)$ or $\phi_{\rm MLR}(r)$ is a (fairly) slowly varying function of r. The MLJ form of Eq. (10) was introduced over a decade ago[42,43] and has been used in a number of demanding data analyses,[46–53] while the MLR form of Eq. (11) is introduced for the first time here. However, it is clear that the latter collapses to the former if $R_{m,n}=0$, so further details regarding both forms are presented below as properties of the MLR form. On the other hand, we retain the two distinct names to simplify the labeling when distinguishing between cases in which two versus one long-range inverse-power terms are incorporated into the potential form.

Since $y_p(r)\to+1$ as $r\to\infty$, at long range the MLR function of Eq. (11) becomes

$$V_{\rm MLR}(r)\simeq \mathfrak{D}_e-\left\{\frac{2\mathfrak{D}_e(r_e)^n e^{-\phi_\infty}}{1+R_{m,n}/r_e^{m-n}}\right\}\left[1+\frac{R_{m,n}}{r^{m-n}}\right]\frac{1}{r^n} \simeq \mathfrak{D}_e-\frac{C_n}{r^n}-\frac{C_m}{r^m}, \quad (12)$$

where $C_n=2\mathfrak{D}_e(r_e)^n e^{-\phi_\infty}/[1+R_{m,n}/r_e^{m-n}]$, $R_{m,n}=C_m/C_n$, and $\phi_\infty\equiv\lim_{r\to\infty}\phi_{\rm MLR}(r)=\ln\{2\mathfrak{D}_e(r_e)^n/(C_n[1+R_{m,n}/r_e^{m-n}])\}$. Thus, the values of the asymptotically dominant long-range potential coefficients C_n and C_m and of $\mathfrak{D}_e$ and r_e define the limiting asymptotic value (ϕ_∞) of the exponent coefficient $\phi_{\rm MLR}(r)$. In order to use the MLR potential form, it is clearly necessary to know appropriate values for n, m, C_n, and

$R_{m,n}=C_m/C_n$ for the species being investigated.

The algebraic form of Eq. (11) means that at sufficiently long range, $V_{\mathrm{MLR}}(r)$ will always eventually collapse to the limiting inverse-power behavior associated with all molecular interaction potentials. The functional form of the exponent coefficient $\phi(r)$ is designed to prevent the potential from having unphysical behavior in the extrapolation interval between the data region and that long-range region.[35,36,43] The present work represents this exponent coefficient by the polynomial function (where MLX means either MLJ or MLR)

$$\phi(r)=\phi_{\mathrm{MLX}}(r)=[1-y_p(r)]\sum_{i=0}^{N}\phi_i y_p(r)^i+y_p(r)\phi_\infty, \quad (13)$$

whose structure means that $\phi(r_e)=\phi_0$ and $\lim_{r\to\infty}\phi(r)=\phi_\infty$. As is the case for an EMO potential, the power series $\Sigma_{i=0}^{N}\phi_i y_p(r)^i$ in Eq. (13) may have different upper bounds of $N=N_S$ and $N=N_L$ for $r\leqslant r_e$ and $r>r_e$, respectively [see Eqs. (8) and (9)].

There is one additional restriction associated with the use of the MLR function of Eq. (11). The polynomial form of our expression for $\phi_{\mathrm{MLR}}(r)$ means that at large r, the leading deviation from the limiting value $(e^{-\phi_\infty})$ of the exponential term in the potential energy function expression is proportional to $1/r^p$. This means that the limiting long-range behavior of $V_{\mathrm{MLR}}(r)$ will only be given by Eq. (12) if the power defining the exponent function expansion variable p is $>(m-n)$. This places a lower bound on the values of p which can be used in an MLR potential function model for a given physical system.

In the following discussion, particular EMO, MLJ, and MLR functions are identified by the order N or the pair of orders N_S and N_L of the polynomial in $y_p(r)$ appearing in Eq. (6) and (13). For models with $N_S=N_L$, only a single integer argument is used, as in $\mathrm{EMO}_p(N)$, while if $N_S\neq N_L$ the label for the model has both orders as arguments, as in $\mathrm{MLR}_p(N_S,N_L)$. Thus, the label $\mathrm{EMO}_2(6)$ refers to an EMO potential with an exponent polynomial of order $N_S=N_L=N=6$ in the expansion variable $y_2(r)$, while $\mathrm{MLR}_4(6,8)$ is an MLR potential defined in terms of the expansion variable $y_4(r)$, whose exponent coefficient has inner and outer polynomial orders of 6 and 8, respectively.

The "adiabatic" and "nonadiabatic" BOB radial functions $\Delta V_{\mathrm{ad}}^{(\alpha)}(r)$ and $g^{(\alpha)}(r)$ are both written as a sum of two terms, one for each component atom, whose magnitudes are inversely proportional to the mass of the particular atomic isotope.[28,32,33,37,54] Since N_2 is electronically homonuclear, in the present case these functions may be written as[36,38]

$$\Delta V_{\mathrm{ad}}^{(\alpha)}(r)=\left(\frac{\Delta M_{\mathrm{N}_a}^{(\alpha)}}{M_{\mathrm{N}_a}^{(\alpha)}}+\frac{\Delta M_{\mathrm{N}_b}^{(\alpha)}}{M_{\mathrm{N}_b}^{(\alpha)}}\right)\widetilde{S}_{\mathrm{ad}}^{\mathrm{N}}(r), \quad (14)$$

$$g^{(\alpha)}(r)=\left(\frac{M_{\mathrm{N}_a}^{(1)}}{M_{\mathrm{N}_a}^{(\alpha)}}+\frac{M_{\mathrm{N}_b}^{(1)}}{M_{\mathrm{N}_b}^{(\alpha)}}\right)\widetilde{R}_{\mathrm{na}}^{\mathrm{N}}(r). \quad (15)$$

As for the Dunham-type BOB parameters $\delta_{l,m}^{(\mathrm{N})}$ discussed in Sec. III, the adiabatic BOB radial function $\widetilde{S}_{\mathrm{ad}}^{\mathrm{N}}(r)$ can be determined only from a simultaneous analysis of data for multiple isotopologues. In a DPF analysis, however, the centrifugal BOB radial function $g^{(\alpha)}(r)$ can, in principle, be determined from an analysis of data for only a single isotopologue.

The potential energy exponent coefficient and the BOB radial functions are both written as power series in the generalized expansion variable $y_p(r)$ of Eq. (7). Following the discussion of Ref. 36, the radial strength functions characterizing the atom-dependent potential energy and centrifugal BOB corrections of Eqs. (14) and (15) are expanded using expressions in which their values at r_e and at the potential asymptote are explicit parameters of the model,

$$\widetilde{S}_{\mathrm{ad}}^{\mathrm{N}}(r)=[1-y_\ell(r)]\sum_{i=0}u_i^{\mathrm{N}}y_p(r)^i+u_\infty^{\mathrm{N}}y_\ell(r), \quad (16)$$

$$\widetilde{R}_{\mathrm{na}}^{\mathrm{N}}(r)=[1-y_p(r)]\sum_{i=0}t_i^{\mathrm{N}}y_p(r)^i+t_\infty^{\mathrm{N}}y_p(r). \quad (17)$$

In particular, their values at r_e are u_0^{N} and t_0^{N}, and their limiting asymptotic values are u_∞^{N} and t_∞^{N}, respectively. The discussion of Ref. 36 shows that $t_\infty^{\mathrm{N}}=0$ for a molecule which dissociates to neutral atoms, and we adopt the Watson convention[32,33] of setting the indeterminate (from transition frequency data alone) parameter $t_0^{\mathrm{N}}=0$. Similarly, defining the zero of energy as the energy of ground-state atoms separated at $r\sim\infty$, $u_\infty^{\mathrm{N}}\equiv 0$ for all electronic states which dissociate to yield ground-state atoms.[36] The parameter u_0^{N} then defines the differences between the well depths of the ground electronic state for different N_2 isotopologues as

$$\delta\mathcal{D}_e^{(\alpha)}=\mathcal{D}_e^{(\alpha)}-\mathcal{D}_e^{(1)}=\left(\frac{\Delta M_{\mathrm{N}_a}^{(\alpha)}}{M_{\mathrm{N}_a}^{(\alpha)}}+\frac{\Delta M_{\mathrm{N}_b}^{(\alpha)}}{M_{\mathrm{N}_b}^{(\alpha)}}\right)u_0^{\mathrm{N}}. \quad (18)$$

However, since the vibrational data for $^{14,14}N_2$ extends only halfway to dissociation and that for $^{15,15}N_2$ extends less than half that far, the small well-depth difference could not be determined from the available experimental data for N_2, so in the present analysis we set $u_0^{\mathrm{N}}=0$.

Another noteworthy point is the choice of the powers p and ℓ characterizing the $y_p(r)$ expansion variables in Eqs. (16) and (17). As was mentioned earlier, setting p at some integer value greater than 1 (say, $p=2-4$) greatly reduces the propensity for a function defined as an expansion in $y_p(r)$ to exhibit spurious behavior at distances outside the radial interval to which the data are sensitive.[35–37] However, there is no reason to require the value of p to be the same for the expansions used to define the potential energy and the BOB radial strength functions.

Finally, we note that at very long range, the factor $[1-y_\ell(r)]\simeq 2(r_e/r)^\ell$. Thus, if the effective radial potential is represented by a MLJ or MLR function, the power ℓ in our expression for $\widetilde{S}_{\mathrm{ad}}^{\mathrm{N}}(r)$, Eq. (16), should be set equal to the power n characterizing the limiting long-range behavior of the potential function itself; this is necessary to ensure that the potential functions for all isotopologues have the same inverse-power limiting long-range functional behavior. This question is, in principle, independent of the choice of the power p used to define the expansion variable of the power

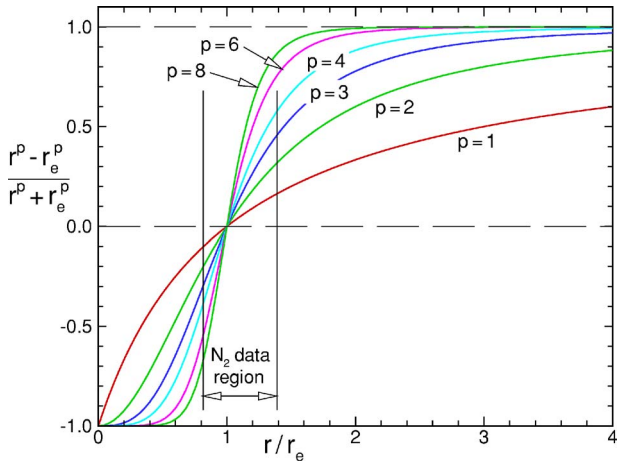

FIG. 1. (Color online) Behavior of the $y_p(r)$ variable for different values of p.

series in Eq. (16). However, when an MLJ or MLR function is used for the potential, it may be convenient also to set the power p used in Eq. (16) equal to $\ell=n$ in order to yield an expression for $\tilde{S}^N_{\rm ad}(r)$ that involves only a single type of expansion variable. Of course, since EMO functions do not have *any* inverse-power limiting long-range behavior, one would always set $\ell=p$ in Eq. (16) when an EMO function is used for the potential energy.

All of the direct potential fits reported herein were performed using the program DPOTFIT, which is freely available on the web, together with a comprehensive program manual.[55] As discussed in the latter, to commence such a nonlinear fit one needs realistic initial trial values of the various potential function parameters. One way of obtaining them is to fit the chosen potential function form to a grid of preliminary potential function values obtained from (say) an RKR inversion procedure[1,31] or from *ab initio* calculations. A companion program (with manual) for performing such preliminary fits is available from that same website.[56] All of the calculations reported herein were performed using isotope masses $m(^{14}\mathrm{N})=14.003\,074\,004\,8$ u and $m(^{15}\mathrm{N})=15.000\,108\,898\,2$ u from Ref. 57 and inertial constant $\hbar^2/2=16.857\,629\,20$ u cm^{-1}Å^2 based on the 2002 values of the physical constants.[58]

B. Nature and importance of the expansion variable

As was mentioned earlier, giving the integer p a value greater than 1 greatly reduces the probability that a function defined as an expansion in $y_p(r)$ will exhibit nonphysical behavior at distances outside the radial interval to which the data are sensitive.[35–37] The reason for this is made clear by considering the plots of $y_p(r)$ for a number of p values shown in Fig. 1. For ground-state N_2, the region in which the data are most sensitive to the nature of the potential function is the interval $r/r_e \in [0.81, 1.39]$ defined by the inner and outer turning points of the highest observed vibrational level, $v=19$. For small values of p, this interval includes only a small fraction of the domain of $y_p(r)$, and it would be unreasonable to expect that a polynomial in $y_p(r)$ determined from a fit to data on this narrow interval would necessarily be "well behaved" (i.e., have no spurious extrema) at small and/or large r outside this region. However, increasing the value of p causes the variable $y_p(r)$ to flatten out and approaches its limiting values of ±1 ever more rapidly, so polynomial functions of such high-p $y_p(r)$ variables will more rapidly approach their limiting constant values outside the data-sensitive region.

The use of relatively large values of p strongly inhibits the irregular behavior of functions of $y_p(r)$ outside the "data region." At the same time, for small values of $|r-r_e|$, $y_p(r) \propto (r-r_e)$ for *all* values of p, so expansions in any of these variables should be able to provide accurate representations for functions of r in the region near r_e. On the other hand, the fact that $y_p(r)$ becomes increasingly "flat" at the edges of the data region with increasing values of p means that associated functions of $y_p(r)$ will become increasingly less able to provide accurate representations of functions of r at large $|r-r_e|$. In practice, this means that for larger values of p, higher-order polynomials in $y_p(r)$ will usually be required to yield an accurate representation of a given function and that, at sufficiently high p, no increase in polynomial order will suffice. Illustrations of these considerations are seen in the results presented below.

C. Results

Although the spectroscopic data considered here span only half of the well depth, an accurate value for the ground-state N_2 dissociation energy, $\mathfrak{D}_e=79\,845\ (\pm 9)$ cm^{-1}, was determined by Roncin *et al.*[59,60] over 20 years ago from an analysis of excited-state predissociation data. Recent independent measurements by Tang *et al.*[61] using the pulsed field-ionization photoelectron-photoion coincidence method yielded an essentially equivalent value of 79 849 (±8) cm^{-1}. Except where stated otherwise, all of the DPFs reported below were performed with $\mathfrak{D}_e$ fixed at the value of Roncin *et al.*[59,60]

The ground electronic state of N_2 dissociates to two ^4S atoms, so the theory of intermolecular forces tells us that the leading contributions to its long-range potential are the attractive inverse-power terms (see Appendix B of Ref. 62 and references therein),

$$V(r) \simeq \mathfrak{D}_e - C_6/r^6 - C_8/r^8 - C_{10}/r^{10} - \cdots . \tag{19}$$

Thus, for the case of an MLJ or MLR potential, the powers appearing in Eqs. (10)–(12) and (16) are $n=l=6$ and $m=8$. To simplify the form of the expression used for $\tilde{S}^{\rm N}_{\rm ad}(r)$, the power p defining the power-series expansion variable in Eq. (16) was set at $p=\ell=6$. However, this had no bearing on the value of p used to define the potential function exponent in Eqs. (6) or (13). Values for $C_6=1.16\times10^5$ cm^{-1} Å^6 and $R_{8,6}=C_8/C_6=5.5$ Å^2 were taken from Meath and co-workers[63,64] and Hettema and Wormer.[65]

Direct potential fits to the data set summarized in Table I were performed using a range of models for the potential energy function and the BOB radial strength functions. Tests showed that the nonadiabatic centrifugal BOB function had no discernible effect on the fit, so the $g^{(\alpha)}(r)$ function of Eqs. (4) and (15) was omitted from further consideration. In con-

TABLE III. Dimensionless rms deviations $\overline{dd}$ for direct potential fits to various model potentials, all performed using one nonzero fitted BOB coefficient u_1^N.

	$N_S=N_L$:	4	5	6	7	8	9	10
EMO	$p=1$	3.58	1.48	1.43	1.43	1.42	⋯	⋯
	$p=2$	6.00	1.44	1.43	1.43	1.42	⋯	⋯
	$p=3$	12.0	2.30	1.45	1.44	1.42	⋯	⋯
	$p=4$	24.5	5.47	1.70	1.56	1.41	⋯	⋯
	$p=5$	48.1	12.1	3.62	2.41	1.45	⋯	⋯
MLJ	$p=1$	14.2	1.46	1.43	1.43	1.42	1.42	⋯
	$p=2$	41.9	3.64	1.59	1.45	1.42	1.42	⋯
	$p=3$	20.4	6.62	3.18	1.74	1.43	1.42	⋯
	$p=4$	⋯	26.3	6.97	1.58	1.42	1.42	1.42
	$p=5$	⋯	⋯	304.	30.5	11.6	3.28	1.52
MLR	$p=3$	⋯	⋯	3.41	1.76	1.44	1.42	1.42
	$p=4$	⋯	⋯	3.05	1.60	1.48	1.43	1.42
	$p=5$	⋯	⋯	⋯	16.6	4.50	1.92	1.41

trast, neglecting of the potential energy BOB function $\Delta V_{\mathrm{ad}}^{(\alpha)}(r)$ increased the dimensionless root mean square deviation of the fits ($\overline{dd}$) by 50%; however, the effect of this term could be fully accounted for by the presence of a single nonzero coefficient u_1^N in Eq. (16).

The dimensionless rms deviations associated with fits to a range of potential function models are shown in Table III. As expected, for a given potential model (i.e., a given value of p and choice of EMO, MLJ, or MLR), increasing the order of the polynomial used to represent the $\phi(r)$ exponent coefficient function causes $\overline{dd}$ to decrease to a limiting value which is essentially the same for all models. Moreover, as predicted by the discussion of Sec. IV B, for a given potential form and $\phi(r)$ polynomial order, the quality of fit generally gets worse as p increases, and for higher-order polynomials the onset of rapid growth in $\overline{dd}$ occurs at relatively higher values of p. Thus, up to a point, good fits could be obtained for models using higher values of p by increasing the order of the exponent polynomial. In addition, although not shown in this table, for a given value of N_L the quality of fit often tends to improve with modest reductions of N_S, since potential well asymmetry means that fewer ϕ_i coefficients are required to accurately define $\phi(r)$ in the relatively narrow portion of the data region with $r \leqslant r_e$. As a result, rather than compete with each other to maintain appropriate physical behavior in the repulsive wall region, the highest-order ϕ_i coefficients are dedicated to defining the potential shape in the broader attractive outer branch of the potential.

Figure 2 compares the potential energy curves associated with several of the best models considered herein; the level energies and turning points shown in the lower segment of this figure indicate the breadth of the data region. It is interesting to note the similarity of these potentials in most of the extrapolation region beyond the outer turning point of the highest level used in the analysis ($v=19$). However, the expanded scale used in the upper segment of this figure shows that there are distinct differences among these potentials at larger distances.

Since they incorporate the correct limiting long-range behavior, an MLJ or MLR potential should, in principle, provide a more realistic description of a long-range potential than would an EMO function. However, the upper segment of Fig. 2 shows that the behaviors of our $MLJ_1(6)$ and $MLJ_2(7)$ functions are very similar to those of the EMO functions shown there. To understand this apparent contradiction, the long-range behavior of the potential must be examined in more detail. Rearrangement of Eq. (19) yields

$$r^6[\mathfrak{D} - V(r)] \simeq C_6 + C_8/r^2 + C_{10}/r^4 + \cdots, \tag{20}$$

and Fig. 3 plots the potential energy functions considered in Fig. 2 in the manner suggested by Eq. (20). Since EMO

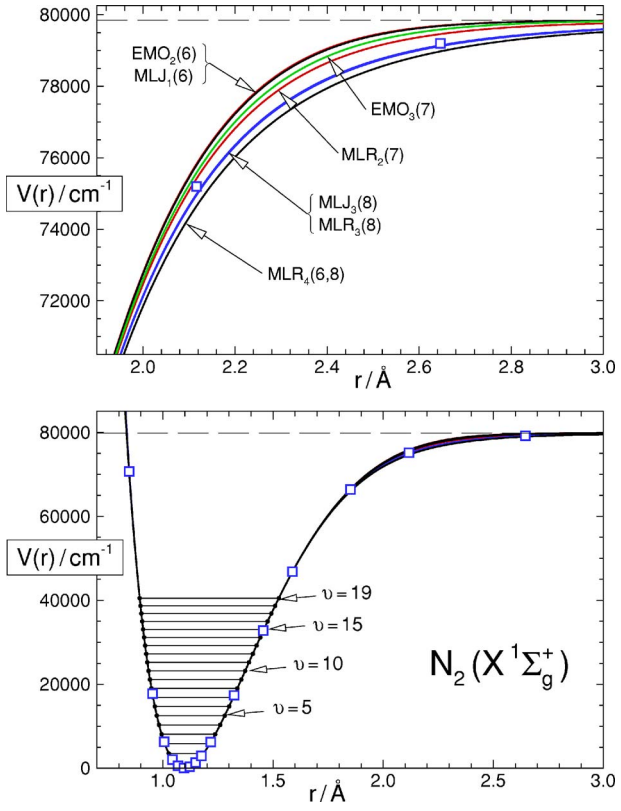

FIG. 2. (Color online) Comparison of several of the fitted potentials listed in Table III. The square open points are the *ab initio* results of Gdanitz (Ref. 3).

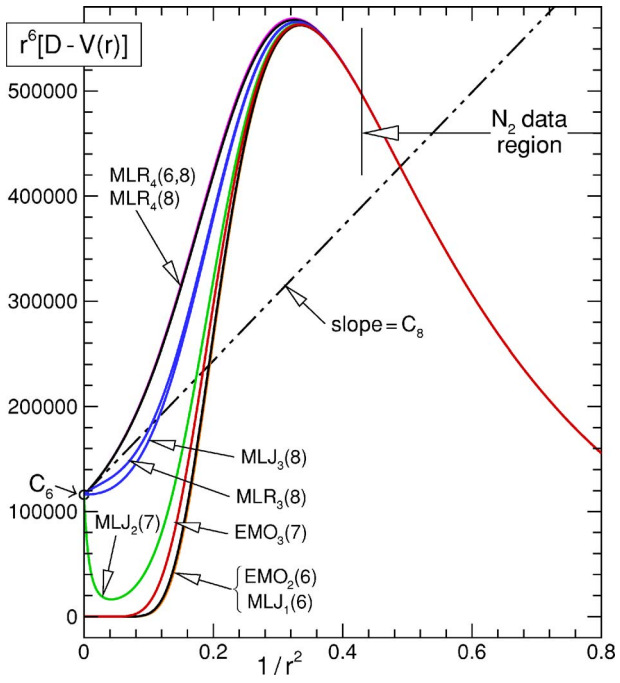

FIG. 3. (Color online) Limiting long-range behavior of the seven fitted potentials considered in Fig. 1.

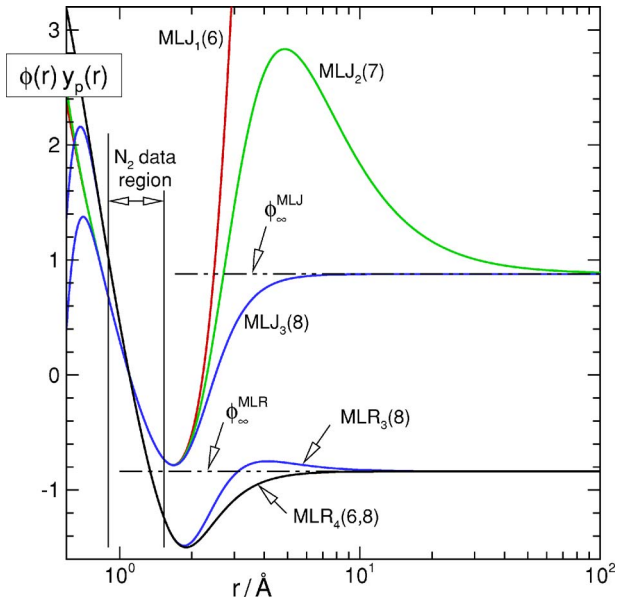

FIG. 4. (Color online) Behavior of the exponents $\phi(r)y_p(r)$ of the fitted MLJ_p and MLR_p potentials considered in Figs. 2 and 3.

potentials have exponential rather than inverse-power long-range behavior, it is no surprise to see that their curves on this plot die off rapidly at small values of $1/r^2$. In contrast, the way the MLJ and MLR potentials for $p=3$ and 4 smoothly approach the limit corresponding to the known (and fixed in the model) C_6 value is qualitatively what we expect from a realistic model potential for this system. In particular, the fact that C_8 and C_{10} are positive (attractive) means that as $(1/r^2)\rightarrow 0$, such curves should approach the C_6 intercept from above. On the other hand, the behavior of the curves yielded by the $\mathrm{MLJ}_1(6)$ and $\mathrm{MLJ}_2(7)$ potentials—dropping to a minimum (of virtually zero for the MLJ_1 function) and only increasing to the intercept of C_6 at very small values of $1/r^2$—is quite unphysical. The reason for that behavior is clearly explained by the plots of the overall exponents of these MLJ potentials shown in Fig. 4.

Figure 4 shows that the exponents of the three MLJ potentials considered in Fig. 3 are essentially identical to one another in the N_2 data region. This is also true for all other MLJ functions which provide accurate fits to the experimental data (see Table III). However, their disparate behavior in the longer-range region shows the importance of the earlier flattening off of the $y_p(r)$ variable for larger values of p shown in Fig. 1. In particular, this relatively rapid flattening off of the $y_3(r)$ expansion variable of the $\mathrm{MLJ}_3(8)$ potential allows its exponent to go smoothly and directly to the asymptotic value of $\phi_\infty^{\mathrm{MLJ}}$ defined by the value of the C_6 coefficient [see discussion following Eq. (12)] without passing through any spurious extremum, and the same is true for all other $p\geqslant 3$ MLJ functions. In contrast, for $p=1$ and 2 the $\phi_{\mathrm{MLJ}}(r)$ functions grow very rapidly outside the data region and only return to the limiting value $\phi_\infty^{\mathrm{MLJ}}$ imposed by their algebraic form at very large r; for $p=1$ this return only occurs at distances $\geqslant$100 Å!

For the MLR potential similar considerations apply. In the extrapolation region the exponent function of the $\mathrm{MLR}_3(8)$ potential "overshoots" the limit and goes through a maximum before dropping back to the limiting value of $\phi_\infty^{\mathrm{MLR}}$ at larger values of r, while those for potentials with $p\geqslant 4$ approach that limit smoothly from below. This correlates with the fact that, as r^{-2} decreases, the $\mathrm{MLR}_3(8)$ curve in Fig. 3 initially drops *below* the limiting slope (equal to C_8) implied by the fixed value of $R_{8,6}$ before taking on that slope very close to the intercept. Such behavior is implausible, since it would imply that the leading deviation from the limiting $\mathfrak{D}_e - C_6/r^8 - C_8/r^8$ potential function behavior is *repulsive*, while theory tells us that all dispersion coefficients are attractive for pairs of ground-state atoms. This "misbehavior" of the MLJ_p potentials for $p\leqslant 2$ and MLR potentials for $p=3$ illustrates the importance of making an appropriate choice for the power p defining the potential energy expansion variable $y_p(r)$. While good fits to data can be achieved more readily for small values of p, attaining physically meaningful behavior in the large-r extrapolation region usually required the use of larger values of p, which in turn tends to require the use of higher-order exponent polynomials.

In summary, Figs. 3 and 4 show that expanding the $\phi(r)$ exponent coefficient of an MLJ potential in terms of a $y_p(r)$ variable corresponding to $p\geqslant 3$ or that for an MLR potential using $p\geqslant 4$ yields a more realistic approach to its theoretically known limiting long-range behavior than is obtained for smaller values of p. Since realistic theoretical values of both C_6 and $R_{8,6}$ are known for ground-state N_2, our fitted MLR potentials for $p\geqslant 4$ are expected to be the most physically realistic. However, when selecting an optimum model potential, other points must be considered. In particular, in addition to having a compact form involving a small number of parameters, we wish to have a potential with no unphysical behavior in the short-range extrapolation region. This latter consideration rules out our fitted $\mathrm{MLR}_4(9)$ and MLR

TABLE IV. Parameters defining the recommended MLR_4 (6,8) potential energy function and BOB radial function for the $X\,^1\Sigma_g^+$ state of N_2; numbers in parentheses are 95% confidence limit uncertainties in the last digits shown. This model yields $\overline{dd}=1.44$. Note that the adiabatic BOB radial function used for this case has the form $\tilde{S}_{ad}^{N}=[1-y_6(r)]u_1^N y_6(r)$.

$\mathfrak{D}_e$	79 845[±9]
$C_6/\mathrm{cm}^{-1}\,\mathrm{Å}^6$	1.16×10^5
$R_{8,6}/\mathrm{Å}^2$	5.5
r_e/Å	1.097 679 (1)
ϕ_0	−2.344 145 47
ϕ_1	−0.972 469
ϕ_2	−1.561 777
ϕ_3	−1.136
ϕ_4	−1.3963
ϕ_5	−0.819
ϕ_6	−0.45
ϕ_7	−3.36
ϕ_8	2.1
u_1^N/cm^{-1}	−14.1(7)

$MLR_5(10)$ potentials, since they happen to have inflection points near 0.76 and 0.85 Å, respectively, and turn over at shorter distances. While this does not occur for the $MLR_4(10)$ potential, it has more parameters that are required to obtain a good fit with this value of p and hence is not as compact as might be possible.

This problem was addressed by allowing the order of the exponent polynomial to be different for $r\leqslant r_e$ and $r>r_e$. As was pointed out earlier, for a given value of N_L, reducing the value of N_S may both reduce the probability of potential function turnover in the short-range region[37] and improve the quality of fit. These considerations led to our choice of an $N_S=6$, $N_L=8$ $MLR_4(6,8)$ potential, for which $\overline{dd}=1.44$, as our recommended potential function for ground-state N_2. The fact that $N_S\neq N_L$ means that at the one point $r=r_e$ there will be small discontinuities in potential function derivatives of order $N_S+2=8$ and higher, but this is a very minor shortcoming. The parameters defining this recommended potential function and the associated fitted value of u_1^N are listed in Table IV. Uncertainties are not listed for the exponent expansion parameters ϕ_i, as they have no individual physical significance.

Finally, Fig. 5 shows the calculated vibrational level spacings and inertial rotational constants for the seven model potentials considered in Figs. 2–4. In view of the differences illustrated by the latter, it is perhaps surprising to see the

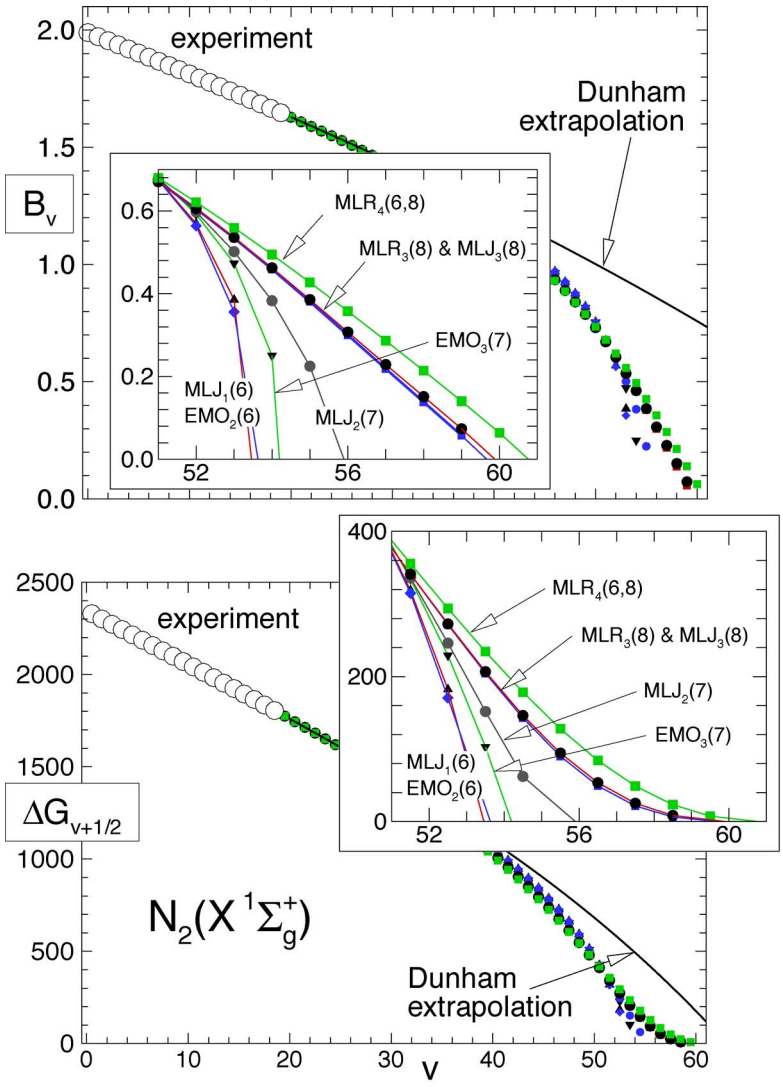

FIG. 5. (Color online) Spectroscopic properties of the seven fitted potentials considered in Figs. 2–4.

similarity of the predicted spectroscopic properties in the "extrapolation region" beyond $v=19$; it is only in the limiting region above $v=50$ that there are substantial differences. The properties of the $MLR_3(8)$, $MLR_4(6,8)$, and $MLJ_3(6)$ potentials all show the limiting near-dissociation behavior predicted by theory:[66,67] positive (quadratic) curvature on the vibrational spacing plot and linear behavior on the B_v plot. While this should also be true for the $MLJ_1(6)$ and $MLJ_2(7)$ potentials, the wayward behavior of their $\phi(r)$ functions at large r means that this limiting behavior would not appear until extremely close to the asymptote, beyond the domain of the discrete bound levels. Our recommended $MLR_4(6,8)$ potential supports 61 vibrational levels, and its dissociation asymptote corresponds to $v_{\mathfrak{D}} \approx 60.8$. For the convenience of interested parties, a listing of the band constants $\{G_v, B_v, -D_v, H_v, \ldots\}$ calculated from this potential for all bound levels of all three N_2 isotopologues is included in supplementary material available from the authors or from the journal's online data archive.[27]

TABLE V. Comparison of fitted $\mathfrak{D}_e$ values obtained using various potential models with the experimental value of 79 845(±9) cm^{-1} (Refs. 59 and 60).

Form	p	N_S, N_L	v_L	$\overline{dd}$	$\mathfrak{D}_e/cm^{-1}$	%error $\{\mathfrak{D}-G(v_L)\}$
EMO	2	6	19	1.43	81 277(±2200)	3.6
	3	7	19	1.42	85 612(±3400)	14.7
MLJ	1	6	19	1.43	79 595(±1200)	0.6
	2	7	19	1.45	85 779(±2800)	15.1
	3	8	19	1.43	83 872(±2100)	10.2
	4	8	19	1.42	79 771(±240)	−0.2
MLR	3	8,8	19	1.44	84 144(±2100)	10.9
	4	6,8	19	1.44	81 432(±510)	4.0
	4	9,9	19	1.43	81 492(±740)	4.2
	5	10,10	19	1.41	79 087(±430)	−1.9
MLR	3	6	10	1.45	83 721(±920)	6.4
	4	6	10	1.45	77 819(±200)	−3.3
	5	8	10	1.42	73 271(±640)	−10.9

V. DISCUSSION AND CONCLUSIONS

One point which deserves comment is the fact that the parameter-fit analysis of Table II gives a slightly better quality of fit than the potential-fit analyses of Table III: $\overline{dd}=1.38$ vs 1.42–1.44. To some degree such differences are expected, since the variables in a parameter-fit analysis usually are not constrained to be consistent with a given Hamiltonian, so values of some of the free parameters may subsume the effects of small systematic errors in the data. Some confirmation of this argument is provided by the fact that in the potential-fit analyses, the linear averages of the dimensionless discrepancies $[v_i^{calc}-v_i^{obs}]/u_i$ for a number of the Raman bands had magnitudes close to those of the corresponding rms averages of these quantities, with the algebraic (±) signs of the difference being different for the $^{14,14}N_2$ and $^{15,15}N_2$ isotopologues. In contrast, in the parameter-fit analysis which allowed for four free $\delta_{l,0}^N$ parameters, the corresponding linearly averaged discrepancies were usually distinctly smaller than their corresponding rms values. This indicates the presence of some small systematic errors in the relative calibration of the vibrational Raman data for the different isotopologues which was artificially hidden by the (nonphysical) extra flexibility of the unconstrained parameter-fit analysis. Note too that since the value of $\overline{dd}=1.44$ associated with our best fits is somewhat greater than unity merely indicates that the estimated experimental uncertainties used to weigh the data were somewhat optimistic.

In previous combined-isotopologue analyses of the CARS data for N_2 by Orlov *et al.*[14] and by Molski,[68,69] the leading parameter in the expression for the BOB correction to the centrifugal potential, t_0^N of Eq. (17), was held fixed at a value based on the magnitude of the rotational g factor $[|g_J|=0.2593(5)\ nm/J]$ determined from molecular beam measurements on $^{15,15}N_2$.[70] This was done in an effort "… to ensure maximal physical significance of the other parameters," even though, as Orlov *et al.*[14] pointed out and was independently confirmed here, "… the fits were insensitive to the presence or absence of t_0^N."[14] On the other hand, Watson has shown that the $\tilde{R}_{na}^N(r)$ function in a Hamiltonian of the form of Eq. (4) contains indeterminate contributions from terms associated with the BOB contribution to the radial kinetic energy operator,[32,33] a fact which muddies the relationship between the rotational g factor and t_0^N. In view of this ambiguity and of the negligible effect of this term on the data, it was omitted from the present analysis.

A somewhat surprising feature of the present potential-fit analysis was the degree of similarity among the results obtained using different types of model potentials, as shown by Figs. 2 and 5. Moreover, when we considered only the data for vibrational levels $v=0-10$ (instead of $v=0-19$), direct potential fits to an analogous range of models yielded potential curves lying essentially within the band of curves shown in Fig. 2! The very modest scale of this "model dependence" mainly reflects the importance of the availability of an accurate experimental value of the dissociation energy (see below) to constrain the extrapolation. However, it also implies that the properties of unobserved levels predicted from our recommended potential energy function[27] should be fairly reliable.

It is interesting to ask how reliable our extrapolations would have been if no accurate experimental dissociation energy were available, and it had been necessary to determine a value of $\mathfrak{D}_e$ from the DPF analysis. To this end, Table V summarizes results of DPF fits to the data for $v=0-v_L$ for $v_L=10$ or 19 using a number of different potential models, with the value of $\mathfrak{D}_e$ being treated as a free parameter. While it is interesting to compare the dissociation energies yielded by these fits with the experimental value of 79 845(±9) cm^{-1},[59,60] it is more relevant to compare the errors in those fitted values of $\mathfrak{D}_e$ with the binding energy of the highest observed level used in the analysis v_L; this is done in the last column of Table V. While it is gratifying to see the small (4%) extrapolation error achieved using our recommended $MLR_4(6,8)$ potential form, it would probably be more appropriate to associate an uncertainty of at least

10%–15% of the binding energy of the highest observed vibrational level with the value of $\mathfrak{D}_e$ determined from this type of fit.

Finally, it is interesting to compare our recommended experimental potential energy curve with theory. It is generally accepted[71] that the most accurate *ab initio* potential for this system reported to date is the r_{12}-MR-ACPF curve reported by Gdanitz;[3] his results are shown as square points in Fig. 2. On the scale of that plot, his results are in excellent agreement with experiment, and the associated dissociation energy is only ca. 129 cm^{-1} too large. If the level spacings and rotational constants calculated from this potential (using the atomic reduced mass) were plotted on Fig. 5, they would be very close to the properties of our recommended $MLJ_4(8)$ potential (round points on Fig. 5). However, the sparseness of the set of *ab initio* potential function values means that interpolation-noise discrepancies in the calculated eigenvalues—the effect of using different methods for interpolating over the function values—ranged from 1 to 7 cm^{-1}. Moreover, differences from the level energies of our recommended potential grow to 35 cm^{-1} by $v=19$ (the upper end of the data region) and up to $\sim$210 cm^{-1} at higher v. However, in view of the challenge addressed in calculating the full potential energy curve for a molecule with a triple bond, the accuracy of Gdanitz's *ab initio* potential[3] is quite remarkable.

In summary, the present work reports combined-isotopologue analyses which provide a set of conventional Dunham-type spectroscopic parameters and an analytic potential function for the ground electronic state of N_2, both of which accurately represent all available vibration-rotation and electronic transition data. While the Dunham-type parameters are not reliable outside the range of the experimental data ($v=0-19$), the recommended $MLR_4(6,8)$ analytic potential should provide reliable predictions at very high J within the vibrational data range, and quite good predictions for $v>19$. Our analysis demonstrates both the considerable power of DPF methods and the important role of the power p in the radial variable $y_p(r)$ for ensuring the optimal physical behavior of the potential function in the large-r extrapolation region. The flexible new MLR potential form introduced here has also proved to provide an effective way of incorporating the correct theoretically known inverse-power long-range behavior on a fitted potential energy function. Our recommended potential energy function should also prove useful for performing accurate quantal calculations of level energies, expectation values, and matrix elements of N_2 required for interpreting atmospheric measurements and modeling.

ACKNOWLEDGMENTS

We are pleased to acknowledge helpful discussions with Professor P. F. Bernath and comments on the manscript by R. D. E. Henderson. This research was supported by the Natural Sciences and Engineering Research Council of Canada, and one of us (C.J.) is also grateful to the University of Waterloo for partial support through a Summer Research Internship.

[1] R. Rydberg, Z. Phys. **73**, 376 (1931); O. Klein, *ibid.* **76**, 226 (1932); R. Rydberg, *ibid.* **80**, 514 (1933); A. L. G. Rees, Proc. Phys. Soc. London **59**, 998 (1947).
[2] K. A. Peterson and T. H. Dunning, Jr., J. Phys. Chem. **99**, 3898 (1995).
[3] R. J. Gdanitz, Chem. Phys. Lett. **283**, 253 (1998).
[4] D. Feller, J. Chem. Phys. **111**, 4373 (1999).
[5] X. Li and J. Paldus, J. Chem. Phys. **113**, 9966 (2000).
[6] F. Rasetti, Nature (London) **123**, 757 (1929).
[7] B. Stoicheff, Can. J. Phys. **32**, 630 (1954).
[8] R. J. Butcher, D. V. Willetts, and W. J. Jones, Proc. R. Soc. London, Ser. A **324**, 231 (1971).
[9] J. Bendtsen, J. Raman Spectrosc. **2**, 133 (1974).
[10] T. R. Gilson, I. R. Beattie, J. D. Black, D. A. Greenhalgh, and S. N. Jenny, J. Raman Spectrosc. **9**, 361 (1980).
[11] B. Lavorel, R. Chaux, R. Saint-Loup, and H. Berger, Opt. Commun. **62**, 25 (1987).
[12] B. Lavorel, G. Millot, M. Lefebvre, and M. Péalat, J. Raman Spectrosc. **19**, 375 (1988).
[13] A. Tabyaoui, B. Lavorel, G. Millot, R. Saint-Loup, R. Chaux, and H. Berger, J. Raman Spectrosc. **21**, 809 (1990).
[14] M. L. Orlov, J. F. Ogilvie, and J. W. Nibler, J. Mol. Spectrosc. **185**, 128 (1997).
[15] J. Bendtsen and F. Rasmussen, J. Raman Spectrosc. **31**, 433 (2000).
[16] J. Bendtsen, J. Raman Spectrosc. **32**, 989 (2001).
[17] D. Reuter, D. E. Jennings, and J. W. Brault, J. Mol. Spectrosc. **115**, 294 (1986).
[18] C. P. Rinsland, R. Zander, A. Goldman, F. J. Murcray, D. G. Murcray, M. R. Gunson, and C. B. Farmer, J. Mol. Spectrosc. **148**, 274 (1991).
[19] D. E. Shemansky, J. Chem. Phys. **51**, 689 (1969).
[20] T. Trickl, D. Proch, and K. L. Kompa, J. Mol. Spectrosc. **162**, 184 (1993).
[21] S. Edwards, J.-Y. Roncin, F. Launay, and F. Rostas, J. Mol. Spectrosc. **162**, 257 (1993).
[22] T. Trickl, D. Proch, and K. L. Kompa, J. Mol. Spectrosc. **171**, 374 (1995).
[23] J.-Y. Roncin, J.-L. Subtil, and F. Launay, J. Mol. Spectrosc. **188**, 128 (1998).
[24] J.-Y. Roncin and F. Launay, Astron. Astrophys., Suppl. Ser. **128**, 361 (1998).
[25] J.-Y. Roncin, F. Launay, H. Bredohl, and I. Dubois, J. Mol. Spectrosc. **194**, 243 (1999).
[26] An additional 11 term values were omitted from the data set because they yielded discrepancies of several cm^{-1} from any realistic model, which indicates the presence of typographical or assignment errors.
[27] See EPAPS Document No. E-JCPSA6-125-014638 for ASCII files containing listings of the data used in the present work, and of the band constant of all vibrational levels of N_2 supported by the present recommended potential energy and BOB radial function. This document can be reached via a direct link in the online article's HTML reference section or via the EPAPS homepage (http://www.aip.org/pubservs/epaps.html).
[28] R. J. Le Roy, J. Mol. Spectrosc. **194**, 189 (1999).
[29] R. J. Le Roy, DParFit 3.3: *A Computer Program for Fitting Multi-Isotopologue Diatomic Molecule Spectra*, University of Waterloo Chemical Physics Research Report No. CP-660, 2005 (unpublished); see http://leroy.uwaterloo.ca/programs/.
[30] R. J. Le Roy, J. Mol. Spectrosc. **191**, 223 (1998).
[31] R. J. Le Roy, RKR1 2.0: *A Computer Program Implementing the First-Order RKR Method for Determining Diatomic Molecule Potential Energy Curves*, University of Waterloo Chemical Physics Research Report No. CP-657, 2003 (unpublished); see http://leroy.uwaterloo.ca/programs
[32] J. K. G. Watson, J. Mol. Spectrosc. **80**, 411 (1980).
[33] J. K. G. Watson, J. Mol. Spectrosc. **223**, 39 (2004).
[34] A. A. Šurkus, R. J. Rakauskas, and A. B. Bolotin, Chem. Phys. Lett. **105**, 291 (1984).
[35] Y. Huang, M.Sc. thesis, University of Waterloo, 2001.
[36] R. J. Le Roy and Y. Huang, J. Mol. Struct.: THEOCHEM **591**, 175 (2002).
[37] Y. Huang and R. J. Le Roy, J. Chem. Phys. **119**, 7398 (2003).
[38] R. J. Le Roy, D. R. T. Appadoo, K. Anderson, A. Shayesteh, I. E. Gordon, and P. F. Bernath, J. Chem. Phys. **123**, 204304 (2005).
[39] E. G. Lee, J. Y. Seto, T. Hirao, P. F. Bernath, and R. J. Le Roy, J. Mol. Spectrosc. **194**, 197 (1999).
[40] J. Y. Seto, Z. Morbi, F. Charron, S. K. Lee, P. F. Bernath, and R. J. Le Roy, J. Chem. Phys. **110**, 11756 (1999).

[41] R. J. Le Roy, D. R. T. Appadoo, R. Colin, and P. F. Bernath, J. Mol. Spectrosc. **236**, 178 (2006).
[42] P. G. Hajigeorgiou and R. J. Le Roy, 49th Ohio State University International Symposium on Molecular Spectroscopy, The Ohio State University, Columbus, Ohio, 1994 (unpublished), paper WE04.
[43] P. G. Hajigeorgiou and R. J. Le Roy, J. Chem. Phys. **112**, 3949 (2000).
[44] In the early work this was called a *modified Lennard-Jones oscillator*, but its algebraic form suggests that *Morse/Lennard-Jones* is probably a more appropriate title.
[45] R. J. Le Roy and R. D. E. Henderson, Mol. Phys. (to be published).
[46] J. A. Coxon and R. Colin, J. Mol. Spectrosc. **181**, 215 (1997).
[47] J. A. Coxon and P. G. Hajigeorgiou, J. Mol. Spectrosc. **193**, 306 (1999).
[48] J. Y. Seto, R. J. Le Roy, J. Vergès, and C. Amiot, J. Chem. Phys. **113**, 3067 (2000).
[49] J. A. Coxon and P. G. Hajigeorgiou, J. Mol. Spectrosc. **203**, 49 (2000).
[50] T. C. Melville and J. A. Coxon, Spectrochim. Acta, Part A **57**, 1171 (2001).
[51] J. Coxon and P. G. Hajigeorgiou, J. Chem. Phys. **121**, 2992 (2004).
[52] J. A. Coxon and C. S. Dickinson, J. Chem. Phys. **121**, 9378 (2004).
[53] J. A. Coxon and T. C. Melville, J. Mol. Spectrosc. **235**, 235 (2006).
[54] J. F. Ogilvie, J. Phys. B **27**, 47 (1994).
[55] R. Le Roy, J. Seto, and Y. Huang, DPotFit 1.0: *A Computer Program for Fitting Diatomic Molecule Spectra to Potential Energy Functions*, University of Waterloo Chemical Physics Research Report No. CP-662, 2006 (unpublished); see http://leroy.uwaterloo.ca/programs/
[56] R. Le Roy, phiFIT 1.1: *A Computer Program to Fit Potential Function Points to Selected Analytic Functions*, University of Waterloo Chemical Physics Research Report No. CP-663R, 2006 (unpublished); see http://leroy.uwaterloo.ca/programs/
[57] G. Audi, A. H. Wapstra, and C. Thibault, Nucl. Phys. A **729**, 337 (2003).
[58] P. J. Mohr and B. N. Taylor, Rev. Mod. Phys. **77**, 1 (2005).
[59] J.-Y. Roncin, F. Launay, and M. Larzillier, Phys. Rev. Lett. **53**, 159 (1984).
[60] This value is 1 cm^{-1} higher than that listed in Ref. 59 because of the improved estimate of the zero point energy used here.
[61] X. Tang, Y. Hou, C. Y. Ng, and B. Ruscic, J. Chem. Phys. **123**, 074330 (2005).
[62] R. J. Le Roy and R. B. Bernstein, J. Chem. Phys. **52**, 3869 (1970).
[63] G. D. Zeiss and W. J. Meath, Mol. Phys. **33**, 1155 (1977).
[64] D. J. Margoliash and W. J. Meath, J. Chem. Phys. **68**, 1426 (1978).
[65] H. Hettema and P. Wormer, J. Chem. Phys. **93**, 3389 (1990).
[66] R. J. Le Roy and R. B. Bernstein, Chem. Phys. Lett. **5**, 42 (1970).
[67] R. J. Le Roy, Can. J. Phys. **50**, 953 (1972).
[68] M. Molski, J. Raman Spectrosc. **30**, 449 (1999).
[69] M. Molski, Phys. Rev. A **60**, 3300 (1999).
[70] S. I. Chan, M. R. Baker, and N. F. Ramsey, Phys. Rev. A **136**, 1224 (1964).
[71] V. Špirko, Collect. Czech. Chem. Commun. **70**, 731 (2005).